Experimental Evaluation of User Influence on Test Zone Size in Multi-probe Anechoic Chamber Setups

Fan, Wei; Kyösti, Pekka; Ji, Yilin; Hentilä, Lassi; Chen, Xiaoming; Pedersen, Gert F.

Published in:
IEEE Access

DOI (link to publication from Publisher):
10.1109/ACCESS.2017.2748558

Publication date:
2017

Document Version
Publisher's PDF, also known as Version of record

IEEE Access
Multidisciplinary | Rapid Review | Open Access Journal

Received August 14, 2017, accepted August 30, 2017, date of publication September 4, 2017,
date of current version September 27, 2017.

Digital Object Identifier 10.1109/ACCESS.2017.2748558

Experimental Evaluation of User Influence on Test Zone Size in Multi-Probe Anechoic Chamber Setups

WEI FAN[1], PEKKA KYÖSTI[2,3], YILIN JI[1], LASSI HENTILÄ[2], XIAOMING CHEN[4], AND GERT FRØLUND PEDERSEN[1]

[1]Antennas, Propagation and Millimeter-wave Systems Section, Department of Electronic Systems, Aalborg University, 9220 Aalborg, Denmark
[2]Keysight Technologies Finland Oy, 90590 Oulu, Finland
[3]Centre for Wireless Communications, University of Oulu, FI-90014 Oulu, Finland
[4]School of Electronic and Information Engineering, Xi'an Jiaotong University, Xi'an 710049, China

Corresponding author: Wei Fan (wfa@es.aau.dk)

This work was supported by the European COST Action IRACON Short-Term-Scientific Mission. The work of W. Fan was supported in part by Danish Council for Independent Research under Grant DFF611100525 and in part by the VIRTUSUO Project through the Innovation Fund Denmark.

ABSTRACT Over-the-air (OTA) radiated testing for multiple-input multiple-output (MIMO) capable mobile terminals has been actively discussed in the standardization in recent years, where multi-probe anechoic chamber (MPAC) method has been selected, together with the radiated two-stage method. The supported test zone size is a key parameter to determine for an MPAC design, and the test zone size is restricted by the number of OTA antennas. A larger test zone would necessitate more OTA antennas, each port of which is driven by an expensive channel emulator radio frequency interface. Results available in the literature are typically limited to free space scenarios, where no user effect in the vicinity of MIMO terminal is present. There is a concern whether or not the test zone size should encompass the user phantom, together with the mobile terminal in the MPAC setup. To address this issue, an extensive measurement campaign was carried out in this paper. Two realistic long term evolution mockups were designed and their performance were evaluated under standard spatial channel models with and without the presence of user phantom. The measurement results have shown that the nearby user phantom can significantly affect the MIMO performance. However, its impact on the test zone size of the MPAC system is negligible, since emulation accuracy in terms of received power, branch power ratio, antenna correlation, and measured throughput under the target and the emulated channels is not affected by the presence of user phantom. Moreover, results measured with the synthetic MPAC method generally match those obtained with the reference two-stage method. These findings are valuable inputs for the ongoing MIMO OTA harmonization work in the standardization.

INDEX TERMS Anechoic chambers, radio propagation, MIMO, testing, antenna arrays.

I. INTRODUCTION

Multiple-input multiple-output (MIMO) technique has been an essential component in modern communication systems such as long term evolution (LTE) and wireless local area network (LAN). It is seen as an enabling technique to improve service of quality in challenging propagation scenarios [1], [2]. Over-the-air (OTA) radiated testing of MIMO capable devices, where built-in internal antennas are used as interface to transmit/receive testing signals, has been intensively discussed in the past few years. The wireless industry, through CTIA and the 3rd Generation Partnership Project (3GPP) standardization bodies, has been working on standard MIMO OTA testing methodologies [3], [4]. Various proposed candidate methodologies differ in the ways to emulate spatial propagation channels with which the multi-antenna terminals are tested [5], [6]. The multi-probe anechoic chamber (MPAC) and the radiated two-stage methods are shown to be capable of emulating arbitrary spatial channel models in principle, and therefore standardized for MIMO device performance testing [3], [4], [6]–[9].

User influence is commonly present in the vicinity of every mobile terminal in true usage conditions. In fact, user

influence, along with propagation environments and antenna designs, determines how well MIMO terminals operate in true usage conditions [10]–[12]. Extensive research works have been reported to assess the user influence on antenna radiation performance, e.g. radiation efficiency and mismatch loss [10]–[12]. It has been recognized that the antenna radiation performance can be greatly degraded in the presence of user influence. Antenna transmit/receive capabilities in terms of total radiated power (TRP) and total isotropic sensitivity (TIS) are required to be evaluated both in free space and with presence of user phantoms in the CTIA OTA testing for single antenna systems [13]. Moreover, CTIA standard has also set guidelines on user interaction with multi-antenna terminals in the MPAC setup [3], [4], [14].

Test zone size is a key parameter to determine in the MPAC design. It is defined as a geometry zone where antennas on the DUT within this zone can not distinguish emulated spatial channels from desired propagation channels. The controlled test zone in any MPAC implementation consisting of a finite number of OTA antennas is defined in terms of the wavelength of the signal. The test zone size supported by an MPAC design is typically determined by the deviation levels in performance metrics under the target scenario and the emulated scenario in the MPAC setup, e.g. field synthesis error in [6], [9], and [15]–[17], spatial correlation error in [6], [9], and [18], capacity error [6], [18] and measured throughput error [19]. A test zone size of 2λ and 0.7λ is determined for the MPAC setup comprised of 16 and 8 uniformly placed probes on the OTA ring based on spatial correlation error in the standards, respectively [3], [4], [20]. As built-in antenna locations on mobile terminals are typically unknown, it is often required that the test zone size should be larger than the physical dimension of the mobile terminal. However, reported works on test zone size determination in the MPAC setup in the literature are generally limited to free space scenarios, where no nearby user effect is present.

Placing a user phantom in the MPAC setup in the vicinity of a MIMO terminal has two effects on MIMO performance: 1) detuning of the antennas by bulky dielectrics, and 2) blocking and scattering of the incoming waves [10]–[12], [14]. The blocking and scattering are expected to introduce reduction of incident power and alter the antenna correlation. Therefore, there is a concern whether the test zone should be large enough to encompass both the MIMO terminal and the user phantom as the DUT in the MPAC setup. This is a critical issue to be addressed, since a larger test zone size would necessitate more OTA antennas (each of which is driven by a channel emulator RF interface port), which would significantly increase the system cost. It is noted that test zone size of an MPAC setup should be distinguished from the quiet zone size of the anechoic chamber. The quiet zone size is determined by the measurement range (distance between OTA antennas and DUT) of the setup. The measurement range R should satisfy $R \geq 2D^2/\lambda$ to ensure that far field assumption is valid, where D is the maximum dimension of the DUT and λ is the wavelength. The quiet zone size should encompass both the MIMO terminal and user phantom in the user-affected scenario, since antenna patterns are altered with the presence of the user phantom. Therefore, introducing the user phantom would require a larger D, which would result in requirement of a larger measurement range in the practical MPAC setup. As discussed, the test zone size is determined by the number of OTA antennas and is an area that propagation channels can be accurately controlled. An MPAC setup with a finite number of OTA antennas has a far smaller test zone than the quite zone of the chamber [4]. The focus of this paper is to investigate whether the test zone size should encompass both the MIMO terminal and the user phantom. In other words, the objective is to investigate whether more probe antennas are needed with the presence of user phantoms in the MPAC setup.

To address this problem, an extensive measurement campaign was performed, where two LTE mockups were designed and evaluated under two standard spatial channel models [21] in the free space scenario and with the presence of user phantom. Two OTA testing methods were adopted in the experiment, i.e. the reference two-stage and the synthetic MPAC method. Emulation accuracy under the target and the emulated channels in terms of received power, branch power ratio (BPR), antenna correlation and measured throughput, is evaluated in the free space and with the presence of user phantom to determine the test zone size.

The paper is structured as below: we explain the problem of determining test zone size for UE terminal in practical MPAC systems with presence of user phantom, and we proposed an equivalent synthetic MPAC system to address the issue in Section II. Antenna pattern measurements in the free space and with the presence of user phantom in a large anechoic chamber are detailed in Section III. After that, Section IV details performance evaluation metrics and simulation results for the target and emulated radio channels. Section V discusses the throughput measurement setup and the measured throughput results and Section VI concludes the paper.

II. PROBLEM STATEMENT AND PROPOSED METHOD

A. INTRODUCTION

1) GEOMETRY BASED STOCHASTIC CHANNEL MODELS

The geometry based stochastic channel (GBSC) models are selected in the study. The widely adopted MIMO channel models like SCME, WINNER and IMT-Advanced models belong to the GBSC family [21], [22]. One advantage of geometry-based modeling is that it enables separation of propagation channels and antennas at the base station (BS) and the user equipment (UE) side. For a MIMO system of S antenna elements at the BS side and U antenna elements at the UE side, the time-variant radio channel transfer function $\mathbf{H}(f,t) \in \mathbb{C}^{U\times S}$ can be written as

$$\mathbf{H}(f,t) = \sum_{n=1}^{N} \mathbf{H}_n(f,t). \quad (1)$$

The (u, s)-th entry of $\mathbf{H}_n(f, t)$ can be expressed as [21]:

$$\begin{aligned} &\mathrm{h}_{u,s,n}(f,t) \\ &= \sum_{m=1}^{M} \begin{bmatrix} g^{V}_{u,UE}(\phi_{n,m}) \\ g^{H}_{u,UE}(\phi_{n,m}) \end{bmatrix}^{T} \begin{bmatrix} \alpha^{VV}_{n,m} & \alpha^{VH}_{n,m} \\ \alpha^{HV}_{n,m} & \alpha^{HH}_{n,m} \end{bmatrix} \begin{bmatrix} g^{V}_{s,BS}(\varphi_{n,m}) \\ g^{H}_{s,BS}(\varphi_{n,m}) \end{bmatrix} \\ &\quad \cdot \exp(j2\pi\vartheta_{n,m}t + \Phi_{n,m}) \exp(-j2\pi f\tau_n), \end{aligned} \tag{2}$$

where $\phi_{n,m}$, $\varphi_{n,m}$, $\vartheta_{n,m}$, $\Phi_{n,m}$ are the angle of arrival, angle of departure, Doppler frequency and initial phase of the m-th subpath of the n-th cluster with $m \in [1, M]$. $\Phi_{n,m}$ is a random variable following the uniform distribution in $[-\pi, \pi]$. τ_n is the delay of the n-th cluster. Coefficient $\alpha^{ab}_{n,m}$ is the complex amplitude of the m-th subpath of the n-th cluster for transmit polarization b and receive polarization a. $g^{V}_{s,BS}$, $g^{H}_{s,BS}$, $g^{V}_{u,UE}$ and $g^{H}_{u,UE}$ are the vertically and horizontally polarized field patterns of the s-th BS antenna element and the u-th UE antenna element, respectively. Note that the antenna field pattern is measured with a common phase reference point, so the spatial signature is included in the field pattern in Eq. 2.

As discussed in Section I, the user influence on radio channels can be split into two parts, i.e. the antenna detuning by bulky dielectrics and the blocking and scattering of incoming waves. The composite effect of these two parts can be fully reflected by the measured antenna patterns with presence of user phantom. Therefore, the channel models with user influence taken into account can be expressed in the same way as in Eq. 2, but the antenna field pattern at the UE side $g^{V}_{u,UE}$ and $g^{H}_{u,UE}$ should refer to those measured with the presence of user phantoms. As shown in Eq. 2, we generated the channel transfer matrix with a composite channel method, which synthetically combines the propagation channels with the measured antenna patterns (with or without presence of user phantoms) [12], [23]. For the user-effected MIMO antenna systems, the user together with the antenna is considered as one radiating unit. This composite channel method was firstly proposed and validated in [12] and [23] and it was typically adopted to evalaute user-affected MIMO antenna systems in the literature, see e.g. in [24] and [25].

The standard SCME urban macro (UMa) tap delay line (TDL) and SCME urban micro (UMi) TDL channel models are selected in the study [21].

2) TWO-STAGE METHOD

An illustration of the conducted testing for MIMO capable terminal is shown in Fig. 1, where the BS emulator is utilized to mimic the BS behavior. The radio CE is used to emulate the radio channel between the BS and the UE. Propagation environments can be mathematically modeled and physically implemented in the CE. The signal model, neglecting the noise, can be expressed as:

$$\boldsymbol{y}(f, t) = \mathbf{H}(f, t)\boldsymbol{x}(f, t), \tag{3}$$

where $\boldsymbol{x}(f, t)$ denotes the transmit signal vector at the BS antenna ports and $\boldsymbol{y}(f, t)$ the testing signal vector received at the UE antenna ports. $\mathbf{H}(f, t)$ is the time-variant radio channel frequency response between the BS antenna ports and the UE antenna ports, as discussed in Eq. (2). The characteristics of the BS antennas and the UE antennas, if known, can be mathematically embedded with the propagation channels [26], as illustrated in Fig 1. This principle is named as the absolute data throughput framework in [20] and [27]. The absolute data throughput frame work was proposed to compare results of different MIMO OTA methodologies with results of conducted testing under the ideal implementation of channel models and UE antennas. The absolute data throughput framework is in principle equivalent to the two-stage method. In the two-stage method, UE antenna patterns are measured in the first stage in an anechoic chamber with a special chipset function support, and the MIMO throughput measurement is performed in the second stage, with measured UE antenna patterns embedded in the propagation channel in the CE [26].

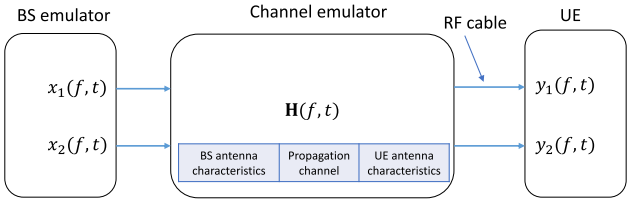

FIGURE 1. A system schematic for 2 × 2 MIMO with conducted two-stage method.

The two-stage method was later extended to the radiated two-stage method [7], [8]. It is noted that the conducted setup is utilized in the study, though the measurements can be done in a radiated setup in principle.

3) MPAC METHOD

An illustration of the MPAC setup is shown in Fig. 2(a). Its equivalent signal model is illustrated in Fig. 2(b) and can be written as:

$$\boldsymbol{y}(f, t) = \mathbf{F}\mathbf{H}_{CE}(f, t)\boldsymbol{x}(f, t) = \hat{\mathbf{H}}(f, t)\boldsymbol{x}(f, t), \tag{4}$$

where $\mathbf{H}_{CE}(f, t)$ is the channel model implemented in the CE, and $\mathbf{F}$ the transfer matrix between the OTA antenna port and the DUT antenna port. $\mathbf{H}_{CE}(f, t)$ is determined from the channel emulation algorithm in the MPAC setup [6], [9], as discussed later. In the practical MPAC system, the transfer matrix $\mathbf{F}$ depends on the OTA antenna, free space propagation in the anechoic chamber and the UE antenna characteristics. $\mathbf{F}$ is typically unknown due to lack of antenna ports on commercial UEs without breaking the device. $\hat{\mathbf{H}}(f, t)$ is the emulated radio channel matrix between the BS antenna port and the UE antenna port. With the MPAC method, internal antennas on the UE are utilized to transmit/receive testing signals, avoiding the cable connection. Channel emulation algorithms in the MPAC setup are extensively discussed in the literature, where the objective is to ensure that the RF signals emitted from the OTA antennas are properly controlled in the CE such that the emulated channels experienced by the DUT approximate the target channel models [6].

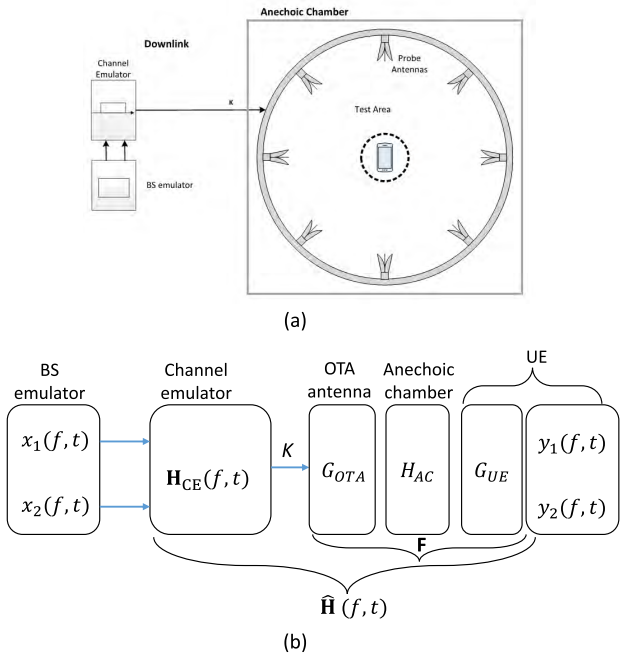

FIGURE 2. (a) A system schematic for 2 × 2 MIMO in the MPAC setup, and (b) block diagram of the signal model. Note that the uplink is neglected in the top figure for simplicity. G_{OTA}, H_{AC}, and G_{UE} denote the OTA antenna characteristics, free space propagation matrix in the anechoic chamber and the UE antenna characteristics, respectively.

In the MPAC setup, omnidirectional antenna patterns are used for the UE antennas in the channel emulation stage (i.e. generation of $\mathbf{H}_{CE}(f,t)$), since the UE antenna pattern is typically not known beforehand. Furthermore, the UE antennas are inherently included in the OTA testing. The channel emulation and the UE antennas are considered separately (as illustrated in Fig. 2(b)), similar to the GBSC principle, where antennas at the BS/UE side and the propagation channel are modeled separately. As a result, $\mathbf{H}_{CE}(f,t)$ is independent of UE antennas, which also indicates that same $\mathbf{H}_{CE}(f,t)$ were emulated (i.e. same signals are emitted from the OTA antennas) in free space scenario and with the presence of user phantom in the MPAC setup. The prefaded signal synthesis (PFS) technique is widely adopted as the channel emulation technique in commercial channel emulators in MPAC setups to obtain $\mathbf{H}_{CE}(f,t)$, due to its simplicity and capability of emulating all dimensions of the GBSC models [9]. With the PFS technique, the (k,s)-th entry for vertically polarized and horizontally polarized probe antenna ports can be expressed as [9]:

$$h_{k,s,n}^{V,CE}(f,t) = \sum_m \begin{bmatrix}1\\0\end{bmatrix}^T \begin{bmatrix}\alpha_n^{VV} & \alpha_n^{VH}\\ \alpha_n^{HV} & \alpha_n^{HH}\end{bmatrix} \begin{bmatrix}g_{s,BS}^V(\varphi_{n,m})\\ g_{s,BS}^H(\varphi_{n,m})\end{bmatrix} \cdot \exp(j2\pi\vartheta_{n,m}t + \Phi_{n,m}) \exp(-j2\pi f\tau_n) \cdot \sqrt{w_{k,n}} \quad (5)$$

$$h_{k,s,n}^{H,CE}(f,t) = \sum_m \begin{bmatrix}0\\1\end{bmatrix}^T \begin{bmatrix}\alpha_n^{VV} & \alpha_n^{VH}\\ \alpha_n^{HV} & \alpha_n^{HH}\end{bmatrix} \begin{bmatrix}g_{s,BS}^V(\varphi_{n,m})\\ g_{s,BS}^H(\varphi_{n,m})\end{bmatrix} \cdot \exp(j2\pi\vartheta_{n,m}t + \Phi_{n,m}) \exp(-j2\pi f\tau_n) \cdot \sqrt{w_{k,n}}, \quad (6)$$

where $w_{k,n}$ denotes the power weight for the k-th probe in the n-th cluster, which can be obtained via optimization algorithms [9]. The objective function in the optimization is to achieve maximum similarity between the emulated discrete power angular spectrum and target power angular spectrum. It is noted that same set of power weight vectors are selected for the vertical polarization and horizontal polarization, since the target incoming power angular spectra are assumed the same for the two polarizations.

B. PROBLEM STATEMENT

As discussed earlier, the test zone size supported by the MPAC setup is determined by the deviation levels in performance metrics under the target channel $\mathbf{H}(f,t)$ and the emulated channel $\hat{\mathbf{H}}(f,t)$. As explained in [19], it is highly desirable that deviation in measured throughput results under $\mathbf{H}(f,t)$ and $\hat{\mathbf{H}}(f,t)$ should be selected as a measure to determine test zone size. Throughput has been selected as the final figure of merit (FoM) in MIMO OTA standards to rank MIMO capable terminal performance, since it reflects the end-user experience [3], [4]. However, it is problematic to use throughput deviation to investigate the impact of user phantom on test zone in the practical MPAC setup. The reasons are multifold:

- Throughput measured under target channel models in the MPAC setup is required as a reference to determine the throughput deviation. However, this is practically not feasible in the MPAC setup, since an infinite number of OTA probes would be required to reproduce the exact target channel models in principle.
- As explained in [19], UE antenna design (e.g. antenna spacing, location and antenna characteristics) and MPAC configuration (e.g. number of OTA probes and measurement range) are fixed in practical MPAC measurement, while test zone size investigation in the MPAC design typically requires flexible MPAC and UE antenna parameter settings.
- Many measurement uncertainties that affect the measured throughput results still exist in practical setups, though extensive efforts have been taken in the MIMO OTA harmonization work in the standardization. For example, the impact of uplink power level and amplifier noise on the measured throughput in the MPAC setup was recently discussed in [28] and [29]. Compared to free space case, the placement of user phantom in the MPAC setup would further increase the system measurement uncertainties.
- It is important to understand why the throughput measured under emulated channels $\hat{\mathbf{H}}(f,t)$ deviates from that measured under target channels $\mathbf{H}(f,t)$ in the free space case and with the presence of user phantom. By analyzing deviation between $\hat{\mathbf{H}}(f,t)$ and $\mathbf{H}(f,t)$ for a DUT in a specific MPAC, it offers more insights on the measured throughput deviation. However, as shown in Fig. 2 (b), $\hat{\mathbf{H}}(f,t)$ is not known due to the fact that $\mathbf{F}$ cannot be obtained in practical MPAC setups.

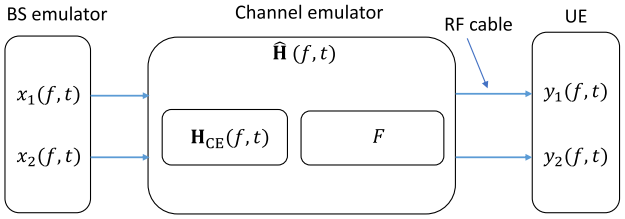

FIGURE 3. A system schematic for 2 × 2 MIMO in the synthetic MPAC setup.

C. SYNTHETIC MPAC METHOD

To address these challenges, we propose to investigate the user influence on test zone size in a synthetic MPAC environment, as illustrated in Fig. 3. Basically, transfer matrix from OTA antenna port to UE antenna port $\mathbf{F}$ can be directly measured, and then mathematically embedded with $\mathbf{H}_{CE}(f,t)$. With the synthetic MPAC method, $\mathbf{F}$ is directly measured, with the help of external LTE mockups. As shown in Fig. 3, internal built-in UE antennas are bypassed in the cable setup and LTE mockup antennas are effectively utilized as external antennas.

The (u, s)-th entry of $\hat{\mathbf{H}}(f,t)$ (i.e. the s-th BS antenna element and u-th UE antenna port) can be calculated analytically, if $\mathbf{F}$ is known, as:

$$\hat{h}_{u,s,n}(f,t) = \sum_{k=1}^{K} g^{V}_{u,UE}(\varphi_k) \cdot h^{V,CE}_{k,s,n}(f,t) + \sum_{k=1}^{K} g^{H}_{u,UE}(\varphi_k) \cdot h^{H,CE}_{k,s,n}(f,t), \quad (7)$$

where φ_k denotes the angular location for the k-th OTA probe in the MPAC setups. $g^{V}_{u,UE}(\varphi_k)$ and $g^{H}_{u,UE}(\varphi_k)$ denote the measured vertically polarized and horizontally polarized fields at angle φ_k for the u-th antenna on the UE. As discussed in Section III, $g^{V}_{u,UE}(\varphi_k)$ and $g^{H}_{u,UE}(\varphi_k)$ are the combined frequency response at frequency f of the OTA antennas, free space propagation inside the anechoic chamber and the u-th UE antenna for a specific direction φ_k for the vertical and horizontal polarization, respectively. It is noted that in the paper the same reference coordinate system was used for the vertical/horizontal polarization directions during the measurement of the UE antenna pattern (with and without user phantom) and the OTA probe pattern.

There are several advantages to investigate the measured throughput in the synthetic MPAC setups. First, same measured throughput results are expected for the practical system and its equivalent synthetic system, since the signal models are the same, as shown in Fig. 2(b)) and Fig. 3. The synthetic MPAC is a derivative of the absolute data throughput framework. As mentioned, the absolute throughput framework is in principle equivalent to the conducted two-stage method. Extensive works have been reported in the MIMO OTA round-robin inter-lab/inter-technique measurement campaign. The absolute data throughput framework was validated in the campaign, where comparable throughput measurement results were reported for the two-stage setup and practical MPAC setup. The synthetic MPAC method was further validated in the throughput measurement in Section V.C in the paper. For test zone size validation purpose, it is desirable that we should avoid potential measurement uncertainties introduced in the MPAC setups. Same measurement setup can be utilized for the reference two-stage method and the synthetic MPAC setup, as shown in Fig. 1 and Fig. 3, respectively (That is, the measurement system consists of the BS emulator, channel emulator and UE with RF cable connections among each equipment). Moreover, throughput can be directly measured under target channel models $\mathbf{H}(f,t)$ and emulated channel models $\hat{\mathbf{H}}(f,t)$, which allows a direct comparison. We have more flexibility in the MPAC design and UE antenna design since $\hat{\mathbf{H}}(f,t)$ is mathematically calculated and loaded in the channel emulator. Further, we can reduce required CE emulator resource in the measurement setup. For example, only two CE output ports are needed in the synthetic MPAC measurement (Fig. 3), compared to 16 CE output ports (i.e. eight dual-polarized OTA antennas) in practical MPAC setups for MIMO capable terminal performance testing required in the standardization [3], [4]. It is noted that end-to-end throughput measurement of MIMO terminals should be carried out in practical MPAC setups. As discussed, in the synthetic MPAC setup, external LTE antennas are measured and embedded with propagation channels in the throughput measurement, with UE built-in antennas bypassed. This method is useful for validation and comparison purpose. However, in the end-to-end performance testing, we are interested in the performance of the UE built-in antennas.

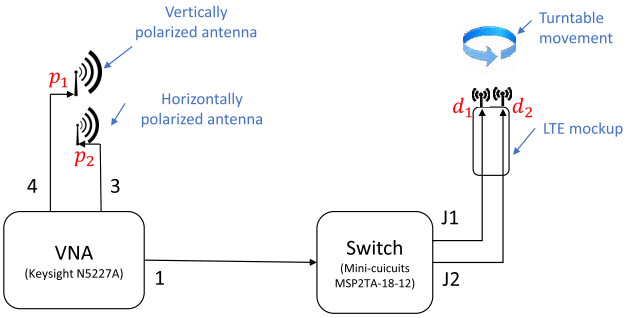

FIGURE 4. Illustration of the system setup for antenna pattern measurements.

III. ANTENNA PATTERN MEASUREMENT WITH AND WITHOUT THE PRESENCE OF USER PHANTOMS

The antenna pattern measurements were performed in a 7 m × 7 m × 10 m anechoic chamber at Aalborg University. An illustration of the measurement system is shown in Fig. 4. The system consists of a three port vector network analyzer (VNA), a single-pole double-throw switch, two probe antennas, an LTE mockup under test and a turntable. The specifications and settings of each component are detailed

TABLE 1. Setup and specifications of each component in the antenna pattern measurement system.

Component	Setup and specifications
VNA	• Model: Keysight N5227A • Complex transmission coefficients $S_{31}(f)$ and $S_{41}(f)$ were recorded from 1 GHz to 3.5 GHz, with 12.5 MHz frequency step, as shown in Fig. 4. That is, a total of 201 frequency points were recorded for each transmission coefficient for each antenna on the LTE mockup under test at each direction.
User phantom	• The user phantom consists of two separate parts, a head phantom and a hand phantom, as shown in Figure 5(b).
Probe antennas	• Two ultra-wideband double-ridged waveguide horn antennas were used, one for the vertical polarization (connected to VNA port 4) and one for the horizontal polarization (connected to VNA port 3). • The two antennas were approximately co-located, with a separation of around 30 cm. The measurement range (i.e. distance between the LTE mockup and horn antenna) is around 5.2 m. • The two probe antennas and the center of the LTE mockup were placed on the same plane, with the help of a laser.
LTE mockups	• Two LTE mockups were investigated, as shown in Fig. 6. • One LTE mockup, detailed in [30], is shown in Fig. 6(a). The mockup consists of two identical small-size multi-band strip monopoles with dimensions $29.5 \times 17 \times 5$ mm^3. The dimensions of the mockup are $124 \times 64 \times 10$ mm^3. The antenna separation is around 0.8λ at $f_c = 1842.5$ MHz. • The other LTE mockup consists of two identical multi-band planar inverted F-antenna (PIFA) elements, as shown in Fig. 6(b). The dimensions of the mockup are $118 \times 56 \times 10$ mm^3. The antenna separation is around 0.7λ at $f_c = 1842.5$ MHz.
Turntable	• The turntable was rotated $P = 360$ steps on the azimuth plane, with 1° per step.

in Table 1. Note that the focus in the study is on the LTE downlink band 3 (i.e. $f_c = 1842.5$ MHz), though measurement data at large bandwidth (i.e. 2.5 GHz) is available.

Antenna patterns in two different modes were measured, free space mode and user influence mode. The free space mode denotes the case where no user is present. This mode is generally adopted for test zone investigation in MPAC setups in the literature, as shown in Fig. 5(a). As for the user influence mode, we focus on the talk mode where the user holds the DUT in the right hand, with top of the LTE mockup pointing to the right ear, as shown in Fig. 5(b). It is noted that special efforts were taken to ensure that LTE mockups were placed to the same location and same orientation in the free space and user influence mode, with the help of a laser. Therefore, the discrepancies in measured antenna patterns in the two modes were only introduced by the effect of user phantom, but not the DUT placement or its orientation. The LTE mockup was 30° slanted in both the free space (with the polystyrene support) and the user influence mode (via adjusting hand phantom placement), as shown in Fig. 5. It is noted that the rotation center coincides with the LTE mockup center during the antenna pattern measurements. A common phase reference point was used throughout the measurement.

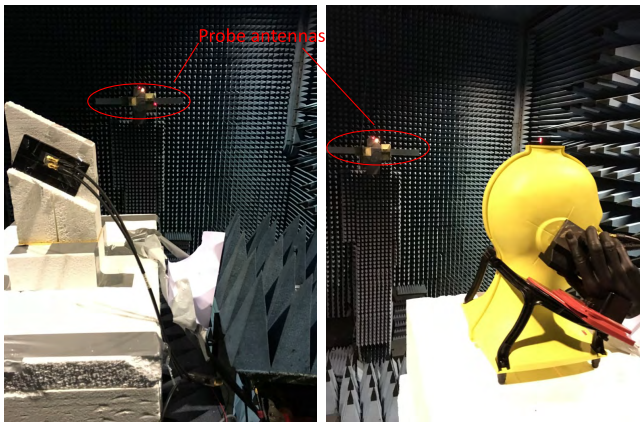

FIGURE 5. A photo of antenna pattern measurement in (a) the free space mode, and (b) the user influence mode.

FIGURE 6. A photo of the two LTE mockups. (a) LTE mockup 1. (b) LTE mockup 2.

RF cables can affect the accuracy of the measured antenna patterns. In the antenna pattern measurement, special efforts were taken to ensure that the cable movement was minimized during the rotation. The cable effect can be further minimized using current chokes (e.g. Ferrite-loaded cable) or replacing the RF cable by optical cables using radio-over-fiber solutions.

A. ANTENNA PATTERN MEASUREMENT PROCEDURE

The calibration was performed first between the antenna ports at the probe antennas and the DUT antennas in a back-to-back manner. As shown in Fig. 4, antenna ports p_1, p_2 were individually connected to d_1 and d_2, and the frequency responses labeled as p_1d_1, p_1d_2, and p_2d_1, p_2d_2, were measured and later calibrated out from the antenna pattern measurement, respectively.

For antenna pattern measurements, the switch was firstly turned to J1 (i.e. with first LTE antenna enabled and second LTE antenna properly terminated). For each turntable orientation, complex transmission coefficients $S_{31}(f)$ and $S_{41}(f)$ were recorded, which correspond to the horizontally

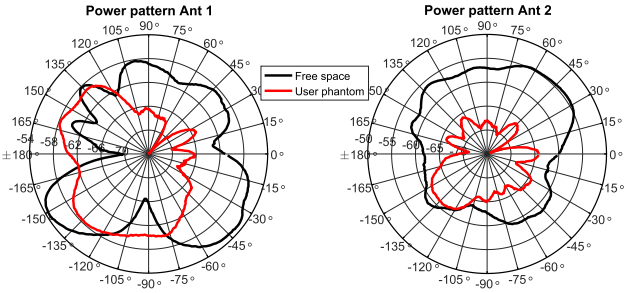

FIGURE 7. The measured total gain patterns of the two antennas on the first mockup in the free space and user influence mode. The radial axis in the polar plot denotes the measured total gain in dB.

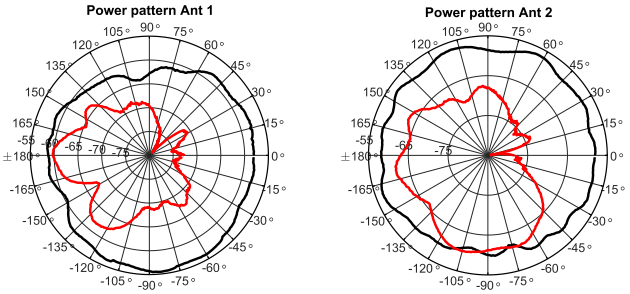

FIGURE 8. The measured total gain patterns of the two antennas on the second mockup in the free space and user influence mode.

polarized and vertically polarized components of the radiation pattern, respectively. Then the same measurements were repeated by setting the switch to J2 to enable the second antenna on the LTE mockup. The measurements were conducted in both the free space mode and the user influence mode. It is noted that only 2D antenna patterns were measured, since 2D channel models are typically seen as sufficient for MIMO OTA performance evaluation at the UE side [3], [4], [20].

B. ANTENNA PATTERN RESULTS

In order to investigate the stability of the measurement system, antenna pattern measurements were repeated at least two times for each antenna. Both the measured phase and gain patterns are highly repeatable, indicating a stable measurement setup. The total gain pattern of the antenna can be calculated as

$$G_{dB} = 10 \cdot \log_{10}(|S_{31}|^2 + |S_{41}|^2) \tag{8}$$

The measured total gain patterns of the two antennas on the first mockup in the free space and the user influence mode are shown in Fig. 7. As we can see, the user phantom has a significant impact on the radiation patterns of the antennas, where widely different antenna patterns are observed in the free space mode and the user influence mode. Further, the antenna radiation performance can be greatly degraded in the presence of user influence. A decrease in the total gain pattern can be typically seen via placing the user phantom in the vicinity of the mockup, despite an increase of the gain can be observed at a few angles. As discussed earlier in Section II-A1, the antenna pattern variation is due to the antenna detuning and blocking of incoming waves introduced by the presence of user phantom. The measured total gain patterns of the two antennas on the second mockup in the free space and the user influence mode are shown in Fig. 8, and similar effects caused by the user phantom on the antenna radiation patterns are observed.

The measured antenna gain pattern per polarization of the two antennas on the first LTE mockup in the free space and the user phantom mode are shown in Fig. 9. Similar to the total gain pattern results, the radiation patterns per polarization are also greatly affected by the presence of user phantom.

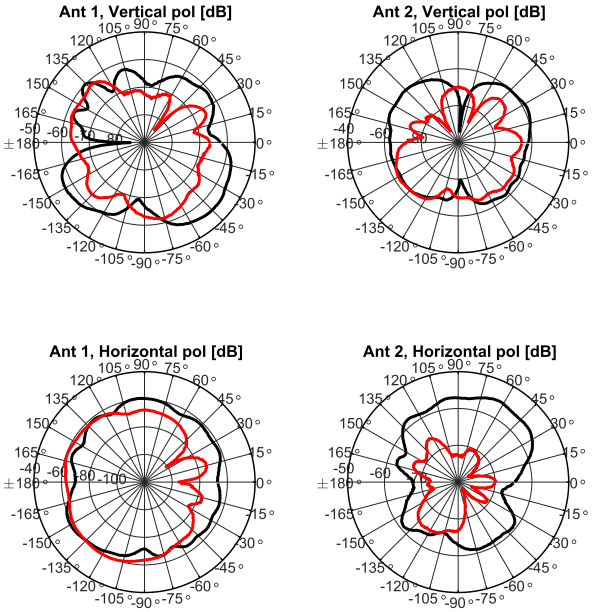

FIGURE 9. The measured gain pattern of the two antennas on the first mockup per polarizations in the free space and user phantom mode.

A gain reduction is typically observed for both polarizations when the user phantom is present, though an increase in gain in few angles is seen as well. The measured gain patterns of the two antennas on the second mockup per polarizations are shown in Fig. 10.

It is noted that the probe antenna, free space propagation in the anechoic chamber, and the DUT antenna are included in the measured field patterns in the study.

IV. SIMULATION RESULTS

A. PERFORMANCE EVALUATION METRICS

Based on the target and the emulated radio channels, we can calculate some other key performance evaluation metrics besides throughput, e.g. the received power at the DUT antenna ports, the BPR between the antenna ports, and the antenna correlation between signals received at the two antenna ports. The channel impulse responses (CIRs) can be directly loaded in the channel emulator, and therefore $\mathbf{H}(\tau, t) = \{h_{u,s,n}(\tau, t)\}$ and $\hat{\mathbf{H}}(\tau, t) = \{\hat{h}_{u,s,n}(\tau, t)\}$ are used for discussion below. It is noted that $\mathbf{H}(f, t)$ and $\mathbf{H}(\tau, t)$, $\hat{\mathbf{H}}(f, t)$ and $\hat{\mathbf{H}}(\tau, t)$ are Fourier transform pairs, respectively.

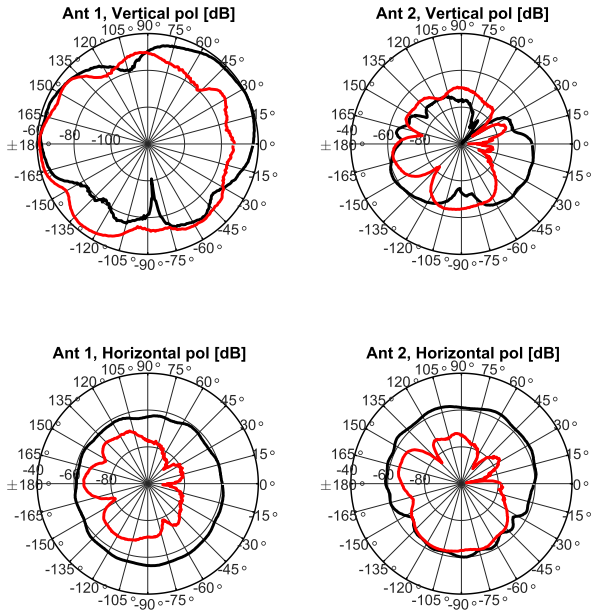

FIGURE 10. The measured gain pattern of the two antennas on the second mockup per polarizations in the free space and user phantom mode.

In our case where we have a 2 × 2 MIMO system with the LTE mockup as the DUT, the average received power for the first and second DUT antenna on the LTE mockup can be calculated as

$$P_1 = \frac{\sum_{t=1}^{N_{ir}} \left|\sum_{\tau=1}^{N_{tap}} h_{11}(\tau,t)\right|^2 + \sum_{t=1}^{N_{ir}} \left|\sum_{\tau=1}^{N_{tap}} h_{12}(\tau,t)\right|^2}{N_{ir}}, \tag{9}$$

$$P_2 = \frac{\sum_{t=1}^{N_{ir}} \left|\sum_{\tau=1}^{N_{tap}} h_{21}(\tau,t)\right|^2 + \sum_{t=1}^{N_{ir}} \left|\sum_{\tau=1}^{N_{tap}} h_{22}(\tau,t)\right|^2}{N_{ir}}, \tag{10}$$

respectively, where N_{tap} denotes the number of taps in delay, and N_{ir} is the number of CIRs in time. The branch power ratio (BPR) can be calculated as

$$\triangle_{\text{dB}} = |10 \cdot \log_{10}(P_1/P_2)|. \tag{11}$$

The antenna correlation between the two DUT antennas can be calculated according to the definition as:

$$\rho_{n_t}^{\text{Rx}} = \text{corr}\left(\sum_{\tau=1}^{N_{tap}} h_{1,n_t}(\tau,t), \sum_{\tau=1}^{N_{tap}} h_{2,n_t}(\tau,t)\right) = \frac{\sum_{t=1}^{N_{ir}} \left[\sum_{\tau=1}^{N_{tap}} h_{1,n_t}(\tau,t) \cdot \sum_{\tau=1}^{N_{tap}} h_{2,n_t}^*(\tau,t)\right]}{\sqrt{\sum_{t=1}^{N_{ir}} \left|\sum_{\tau=1}^{N_{tap}} h_{1,n_t}(\tau,t)\right|^2 \cdot \sum_{t=1}^{N_{ir}} \left|\sum_{\tau=1}^{N_{tap}} h_{2,n_t}(\tau,t)\right|^2}}, \tag{12}$$

Note that $\rho_1^{\text{Rx}} = \rho_2^{\text{Rx}}$ are expected if same radiation patterns for the BS antennas are specified [31]. In this study, two co-located dipole antennas with a ±45° slanted configuration are selected for the BS antennas, same as in the MIMO OTA standard [3], [4]. Therefore, we have $\rho_1^{\text{Rx}} = \rho_2^{\text{Rx}}$. It is noted that the discussed evaluation metrics for the emulated channels can be obtained via replacing $h_{n_r,n_t}(\tau,t)$ by respective $\hat{h}_{n_r,n_t}(\tau,t)$.

B. SIMULATION RESULTS

1) FIRST LTE MOCKUP

The average received power for the two antennas on the first LTE mockup are shown in Table 2 for both the free space mode and user phantom mode. The received power P_1 and P_2 depend highly on the propagation channels and the DUT usage mode. A significant reduction in the received power P_1 and P_2 on the two antennas in the presence of user phantom was observed compared to free space conditions. A reduction up to approximately 4 dB for the P_1 and 12 dB for P_2 in the UMa channel are observed, while 6 dB for the P_1 and 8.5 dB for P_2 in the UMi channel, respectively. The BPR depends highly on the propagation channels and DUT usage mode as well. For example, received power P_2 is higher than P_1 in the free space mode for both channel models, while P_2 is smaller than P_1 in the user influence mode for both channel models. That is the BPR can be either reduced or increased, depending on the channel models and usage mode.

TABLE 2. Average received power and branch power ratio for the target and emulated ($K = 8$ and $K = 16$) channel models for the first mockup antenna in the free space mode and user influence mode.

		Free space			User phantom		
		P_1 [dB]	P_2 [dB]	Δ [dB]	P_1 [dB]	P_2 [dB]	Δ [dB]
UMa	$K = 8$	−2.4	1.8	4.2	−6.9	−10.4	3.5
	$K = 16$	−2.8	1.8	4.6	−6.8	−10.3	3.5
	Target	−2.8	1.9	4.7	−7.0	−10.5	3.5
UMi	$K = 8$	0.8	1.4	0.6	−5.1	−6.6	1.5
	$K = 16$	1.2	1.6	0.4	−4.9	−6.8	1.9
	Target	1.2	1.4	0.2	−5.2	−7.1	1.9

The received power P_1, P_2 and BPR under the emulated channel models generally agree well with that under the target channel models, both in the free space mode and the user phantom mode. As we can see, with $K = 8$ probe antennas, a deviation up to 0.4 dB for P_1 and 0.5 dB for P_2 are observed. With $K = 16$ probe antennas, a better match in the received power P_1, P_2 and BPR under target and emulated channel models can be observed, with a deviation up to 0.3 dB. As a summary, the measured results indicate that the presence of user phantom has a negligible impact on emulation accuracy with respect to the total received power and BPR.

The measured antenna correlations under the target and emulated ($K = 8$ and $K = 16$) channel models for the first mockup antenna are shown in Fig. 11 (left) for the free space mode and in Fig. 11 (right) for the user phantom mode, respectively. The presence of user phantom can either correlate the received signals (as for the UMi model) or de-correlate the received signals (as for the UMa channels). However, the antenna correlation under the emulated channel models agree well with that under the target channel models,

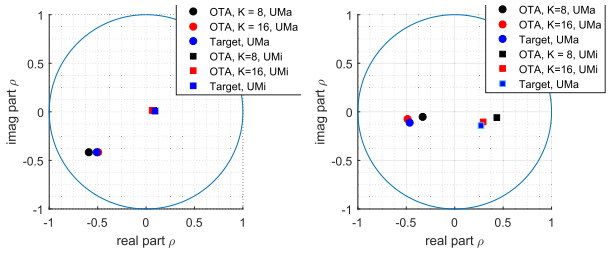

FIGURE 11. Measured antenna correlation for the target and emulated ($K = 8$ and $K = 16$) channel models for the first mockup antenna in the free space mode (left) and user influence mode (right).

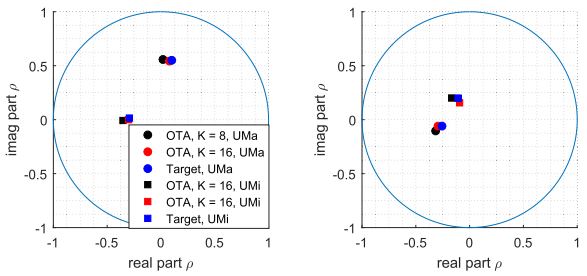

FIGURE 12. Measured antenna correlation for the target and emulated ($K = 8$ and $K = 16$) channel models for the second mockup antenna in the free space mode (left) and user influence mode (right).

both in the free space and in the user phantom mode. With $K = 8$ probe antennas, a deviation up to 0.15 can be observed for all cases between the measured and target channel models. With $K = 16$, a better match is generally achieved for all cases, as expected.

2) SECOND LTE MOCKUP

The received power and BPR for the target and emulated ($K = 8$ and $K = 16$) channel models for the second mockup antenna are shown in Table 3. Similar to the first LTE mockup, a significant power reduction in P_1 and P_2 in the presence of user phantom can be observed, with a reduction up to approximately 11 dB for the P_1 and 12.5 dB for P_2 in the UMa channel, while 12 dB for the P_1 and 10 dB for P_2 in the UMi channel, respectively. The received power P_1, P_2 and BPR under the emulated channel models generally agree very well with those under the target channel models. As we can see, with $K = 8$ probe antennas, a deviation up to 0.9 dB for P_1 and 1 dB for P_2 were observed. With $K = 16$ probe antennas, the deviation is up to 0.3 dB in all cases, indicating a better channel emulation accuracy, as expected.

TABLE 3. Average received power and branch power ratio for the target and emulated ($K = 8$ and $K = 16$) channel models for the second mockup antenna.

		Free space			User phantom		
		P_1 [dB]	P_2 [dB]	Δ [dB]	P_1 [dB]	P_2 [dB]	Δ [dB]
UMa	$K = 8$	-1.6	0.3	1.9	-12.0	-12.6	0.6
	$K = 16$	-1.8	0.8	2.6	-12.9	-11.6	1.3
	Target	-1.8	0.8	2.6	-12.9	-11.6	1.3
UMi	$K = 8$	1.3	1.0	0.3	-9.7	-9.2	0.5
	$K = 16$	1.4	1.4	0	-10.5	-8.7	1.8
	Target	1.5	1.0	0.5	-10.4	-8.8	1.6

For the second LTE mockup, the measured antenna correlation depends highly on propagation channels and the usage mode, similar to results for the first LTE mockup. Again, the antenna correlation under the emulated channel models agree well with that under the target channel models, both in the free space and in the user influence mode. With $K = 8$ probe antennas, a deviation less than 0.1 can be observed for all cases between the measured and target channel models.

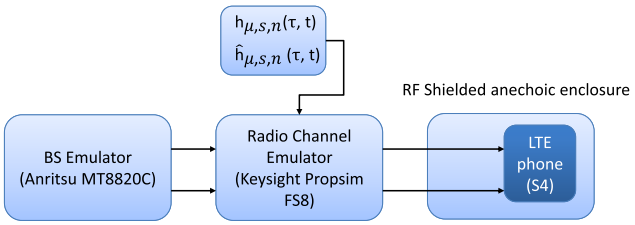

FIGURE 13. Illustration of the throughput measurement setup in the study.

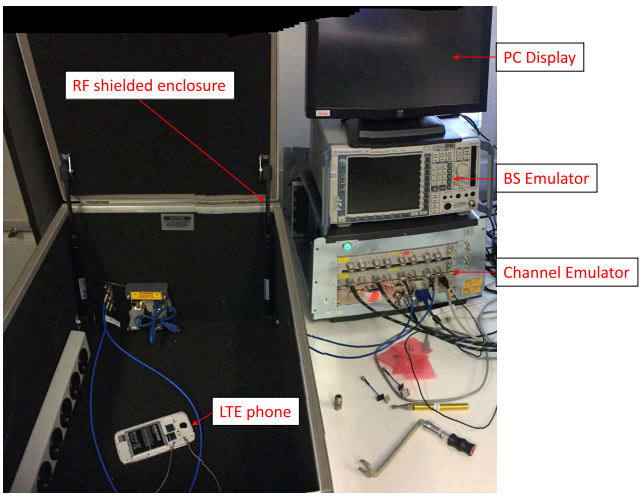

FIGURE 14. Photo of the practical setup for throughput measurement.

V. THROUGHPUT MEASUREMENT AND RESULT ANALYSIS

A. MEASUREMENT SETUP

The throughput measurement setup is illustrated in Fig. 13, where the system consists of a BS emulator, an radio CE, an RF shielded anechoic enclosure and an LTE phone. The specification of each component is detailed in Table 4. A photo of the measured DUT in an RF shielded enclosure is shown in Figure 14. The basic idea is to investigate measured throughput results under target and the emulated channels in the free space case and with the presence of user phantom.

TABLE 4. Setup and specifications of each component in the measurement system.

Component	Setup and specifications
BS emulator	• Model: Anritsu MT8820C • Modulation and coding (MCS) index: 13 • Frame structure: frequency division duplex (FDD) • LTE frequency band: 3 • Channel bandwidth: 10 MHz • Transmission mode: 2 × 2 open loop MIMO
Radio channel emulator	• Model: Keysight Propsim FS 8 • BS array: 2 co-located elements with ±45° slanted configuration, as detailed in [3], [4]. • Channel models: Target and emulated dual polarized SCME UMi and UMa channel models. • OTA configuration for emulated channels: a uniform MPAC setup with eight probe antennas. • MS array: measured antenna patterns in free space or in the presence of user phantom, as detailed in Section III.
MS	• Model: Sumsung Galaxy S4

B. MEASUREMENT PROCEDURE

The throughput measurement procedure is detailed in [3]. Note that the interference and noise are not modeled in the measurement for simplicity. In typical throughput measurement procedure, we adjusted the attenuators in the channel emulator output port to achieve reference signal received power (RSRP) values required for maximum throughput for each loaded channel models. However, this is problematic for our analysis. As discussed in IV-B, the received power values in different channel models and in different usage modes are different. This power difference would be effectively altered if different attenuation values were selected in the CE. To avoid this, a common attenuation factor, which allows maximum throughput for the worse case, was selected for all measurements.

For each throughput measurement point, the RSRP values were decreased with a 2 dB step until the LTE throughput reaches below 10% of the maximum throughput. For each throughput measurement point, 20000 subframes per stream were utilized, as suggested in [3]. A total of eight throughput curve measurements were performed with two usage modes (i.e. free space and user phantom), two channel models (i.e. UMa and UMi), and two channel conditions (i.e. target and emulated with $K = 8$ OTA antennas). It is noted that the throughput measurements under the emulated channels with $K = 16$ OTA antennas were not carried out, since excellent agreement was achieved with $K = 8$ OTA antennas, as explained later.

C. MEASUREMENT RESULTS

The measured throughput curves under the target and the emulated (with $K = 8$) channel models for the first LTE mockup in the free space mode and the user phantom mode are shown in Fig. 15. The measured throughput results depend on the antenna correlation, branch power ratio and received power, as expected [32]. The measured throughput results for the target UMa models in free space are generally much lower than those for target UMi models in free space, with a difference up to 9 dB in RSRP at 70% maximum throughput values. This is due to the fact that UMa channel models are ill-conditioned. In the free space case, as shown in Section IV-B, the UMa channel presents BPR about 4.7 dB, whereas the BPR of the UMi is only 0.2 dB and the UMa has a very high correlation (about 0.96 at the BS and 0.66 at the UE), whereas UMi has very low correlation (below 0.1 at both sides). As for the user phantom case, besides the correlation difference at the BS side, a larger BPR is also present in the UMa channel, compared to the UMi channel.

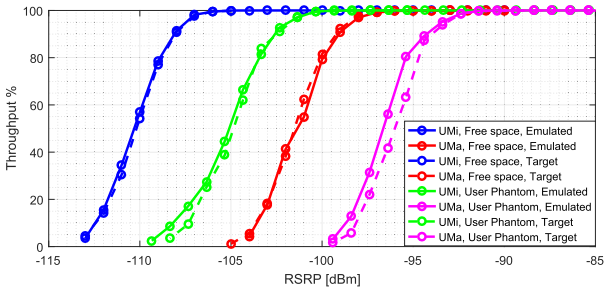

FIGURE 15. The measured throughput results under the target and emulated (with $K = 8$) channel models for the first LTE mockup in the free space mode and user influence mode.

The measured throughput results for both target channel models with presence of user phantoms are generally much lower than those in free space mode, with a difference up to 4.5 dB in RSRP at 70% maximum throughput values. This is mainly due to the fact that a significant received power reduction introduced by the user phantom.

An excellent agreement between measured throughput under target and the emulated channels can be seen for all cases, with a deviation less than 0.5 dB in RSRP at 70% maximum throughput values. The excellent agreement in the measured throughput is expected, since a good emulation accuracy in terms of received power, BPR and antenna correlation is achieved for all cases, as discussed in Section IV-B.

VI. CONCLUSION

In this paper, the impact of user phantom on the MIMO terminal performance and test zone size in the MPAC system is experimentally investigated. The user phantom has a significant impact on the radiation patterns of the antennas. Widely different antenna patterns are observed in the free space mode and with the presence of the user phantom. Further, the antenna radiation performance can be greatly degraded in the presence of user phantom, due to the antenna detuning and blocking of incoming fields with the user phantom. The received power of the LTE antennas depend highly on the propagation channels and DUT operation mode. A significant reduction in the received power (from 4 dB to 12.5 dB) on the two DUT antennas was observed in the presence of user phantom, compared to free space conditions. BPR can be either reduced or increased with presense of phantom, depending on the channel models and the LTE mockup

under testing. Moreover, the presence of user phantom can either correlate or de-correlate the received signals. The measured throughput results for both target channel models with presence of user phantoms are generally much lower than those in free space mode, with a difference up to 4.5 dB in RSRP at 70% maximum throughput values. This is mainly due to the fact that a significant received power reduction introduced by the user phantom.

The impact of user phantom on the test zone size is not noticeable in the study. The deviations in terms of received power, BPR, antenna correlation and measured throughput under the target and emulated channel models are not noticeably affected by the presence of the user phantom. The deviation in received power is up to 0.4 dB under target channel and the emulated channel for LTE mockup 1 in the free space and up to 0.5 dB in the user phantom mode, respectively. As for LTE mockup 2, the deviation is up to 0.5 dB and 1 dB for the free space and the user phantom mode, respectively. The deviation in BPR is 0.5 dB under target channel and emulated channel for LTE mockup 1 in the free space and up to 0.5 dB in the user phantom mode, respectively. As for mockup 2, the deviation is up to 0.7 dB and 1.1 dB, respectively. The deviations in measured antenna correlation under target channel and emulated channel are up to 0.15 in free space and user phantom mode for both LTE mockups. The deviation in measured throughput is less than 0.5 dB in RSRP at 70% maximum throughput value in free space and user phantom mode for LTE mockup 1.

As a summary, the test zone size in the MPAC setup is not altered with presence of a nearby user phantom. Therefore, introducing a user phantom does not require higher number of OTA antennas in the MPAC setup. However, it is noted that introducing the user phantom requires larger measurement range in the MPAC setup. The measurement range should be sufficiently large to ensure that the quiet zone of the anechoic chamber should encompass both the user terminals and the user phantom. This is to ensure the antenna patterns can be accurately measured with the presence of user phantom.

In this paper, we experimentally evaluated the impact of user phantom on test zone size in the MPAC setups, adopting a synthetic MPAC framework. To further validate the work in the future work, throughput results measured under the same channel model in the practical MPAC setup and the radiated two-stage setup should be compared, both in the free space scenario and with presence of user phantom. This extensive round-robin measurement campaign involving user phantom in the test setup would require joint effort in the community.

ACKNOWLEDGMENT

The authors appreciate Mr. Stanislav Stefanov Zhekov with Aalborg University and Mr. Simon Stanev with Wispry for providing the LTE mockups. The authors appreciate the help in the practical measurements from Mr. Kristian Bank. The work was inspired by a critical comment from an anonymous reviewer of a manuscript submitted to IEEE AWPL letter, and the authors highly appreciate the comment.

REFERENCES

[1] R. He *et al.*, "High-speed railway communications: From GSM-R to LTE-R," *IEEE Veh. Technol. Mag.*, vol. 11, no. 3, pp. 49–58, Sep. 2016.

[2] B. Ai *et al.*, "Future railway services-oriented mobile communications network," *IEEE Commun. Mag.*, vol. 53, no. 10, pp. 78–85, Oct. 2015.

[3] *Verification of Radiated Multi-Antenna Reception Performance of User Equipment (UE)*, document 3GPP TR 37.977 V14.0.0, 3rd Generation Partnership Project, Jun. 2016.

[4] "Test plan for 2×2 downlink MIMO and transmit diversity over-the-air performance," CTIA Certification, Washington, DC, USA, Tech. Rep. Version 1.1, Aug. 2016.

[5] X. Chen, "Throughput modeling and measurement in an isotropic-scattering reverberation chamber," *IEEE Trans. Antennas Propag.*, vol. 62, no. 4, pp. 2130–2139, Apr. 2014.

[6] W. Fan, X. Carreno, P. Kyosti, J. O. Nielsen, and G. F. Pedersen, "Over-the-air testing of MIMO-capable terminals: Evaluation of multiple-antenna systems in realistic multipath propagation environments using an OTA method," *IEEE Veh. Technol. Mag.*, vol. 10, no. 2, pp. 38–46, Jun. 2015.

[7] Y. Jing, H. Kong, and M. Rumney, "MIMO OTA test for a mobile station performance evaluation," *IEEE Instrum. Meas. Mag.*, vol. 19, no. 3, pp. 43–50, Jun. 2016.

[8] W. Yu, Y. Qi, K. Liu, Y. Xu, and J. Fan, "Radiated two-stage method for LTE MIMO user equipment performance evaluation," *IEEE Trans. Electromagn. Compat.*, vol. 56, no. 6, pp. 1691–1696, Dec. 2014.

[9] P. Kyösti, T. Jämsä, and J.-P. Nuutinen, "Channel modelling for multi-probe over-the-air MIMO testing," *Int. J. Antennas Propag.*, vol. 2012, Mar. 2012, Art. no. 615954, doi: 10.1155/2012/615954.

[10] I. Vasilev and B. K. Lau, "On user effects in MIMO handset antennas designed using characteristic modes," *IEEE Antennas Wireless Propag. Lett.*, vol. 15, pp. 758–761, 2016.

[11] M. Pelosi, O. Franek, M. B. Knudsen, M. Christensen, and G. F. Pedersen, "A grip study for talk and data modes in mobile phones," *IEEE Trans. Antennas Propag.*, vol. 57, no. 4, pp. 856–865, Apr. 2009.

[12] F. Harrysson, J. Medbo, A. F. Molisch, A. J. Johansson, and F. Tufvesson, "Efficient experimental evaluation of a MIMO handset with user influence," *IEEE Trans. Wireless Commun.*, vol. 9, no. 2, pp. 853–863, Feb. 2010.

[13] *Test Plan for Wireless Device Over-the-Air Performance*, CTIA Certification Program, Washington, DC, USA, Jun. 2017.

[14] X. Wu, N. Wang, Z. Zhang, N. Kuster, and W. Wang, "Comparison tests and hand phantom standardization for multi-probe based MIMO OTA," in *Proc. IEEE 5th Asia–Pacific Conf. Antennas Propag. (APCAP)*, Jul. 2016, pp. 321–322.

[15] J. T. Toivanen, T. A. Laitinen, V. M. Kolmonen, and P. Vainikainen, "Reproduction of arbitrary multipath environments in laboratory conditions," *IEEE Trans. Instrum. Meas.*, vol. 60, no. 1, pp. 275–281, Jan. 2011.

[16] W. A. T. Kotterman, A. Heuberger, and R. S. Thoma, "On the accuracy of synthesised wave-fields in MIMO-OTA set-ups," in *Proc. 5th Eur. Conf. Antennas Propag. (EUCAP)*, Apr. 2011, pp. 2560–2564.

[17] W. A. T. Kotterman, M. Landmann, A. Heuberger, and R. S. Thoma, "New laboratory for over-the-air testing and wave field synthesis," in *Proc. 30th URSI Gen. Assembly Sci. Symp.*, Aug. 2011, pp. 1–4.

[18] A. Khatun *et al.*, "Experimental verification of a plane-wave field synthesis technique for MIMO OTA antenna testing," *IEEE Trans. Antennas Propag.*, vol. 64, no. 7, pp. 3141–3150, Jul. 2016.

[19] W. Fan, L. Hentilä, P. Kyösti, and G. F. Pedersen, "Test zone size characterization with measured MIMO throughput for simulated MPAC configurations in conductive setups," *IEEE Trans. Veh. Technol.*, to be published.

[20] *Verification of Radiated Multi-Antenna Reception Performance of User Equipment (UE)*, document 3GPP TR 37.977 V14.3.0, 3rd Generation Partnership Project, Mar. 2017.

[21] *Spatial Channel Model for Multiple Input Multiple Output (MIMO) Simulations*, document 3GPP TR 25.996 V13.0.0, 3rd Generation Partnership Project, Dec. 2015.

[22] J. Meinilä, P. Kyösti, T. Jämsä, and L. Hentilä, "WINNER II channel models," WINNER II, Tech. Rep. D1.1.2 V1.2. IST-4-027756, Sep. 2007.

[23] F. Harrysson, J. Medbo, A. F. Molisch, A. J. Johansson, and F. Tufvesson, "The composite channel method: Efficient experimental evaluation of a realistic MIMO terminal in the presence of a human body," in *Proc. IEEE Veh. Technol. Conf. VTC Spring*, May 2008, pp. 473–477.

[24] S. M. Ali, A. Mobasher, and P. Lusina, "User effects on MIMO performance: From an antenna to a link perspective," *Int. J. Antennas Propag.*, vol. 2011, Jun. 2011, Art. no. 918315, doi: 10.1155/2011/918315.

[25] S. Myllymaki and M. Berg, "Sensing the human user as a part of multiple-antenna system design [wireless corner]," *IEEE Antennas Propag. Mag.*, vol. 54, no. 5, pp. 231–237, Oct. 2012.
[26] Y. Jing, X. Zhao, H. Kong, S. Duffy, and M. Rumney, "Two-stage over-the-air (OTA) test method for LTE MIMO device performance evaluation," *Int. J. Antennas Propag.*, vol. 2012, Mar. 2012, Art. no. 572419, doi: 10.1155/2012/572419.
[27] I. Szini, G. F. Pedersen, A. Scannavini, and L. J. Foged, "MIMO 2 × 2 reference antennas concept," in *Proc. 6th Eur. Conf. Antennas Propag. (EUCAP)*, Mar. 2012, pp. 1540–1543.
[28] *Noise Issues in MPAC System*, document 3GPP TSG-RAN WG4 R4-1704751, 3rd Generation Partnership Project, May 2017.
[29] *Uplink Power Control for MIMO OTA*, document 3GPP TSG-RAN WG4 R4-1703730, 3rd Generation Partnership Project, Apr. 2017.
[30] S. S. Zhekov, A. Tatomirescu, and G. F. Pedersen, "Compact multi-band sensing MIMO antenna array for cognitive radio system," in *Proc. Loughborough Antennas Propag. Conf. (LAPC)*, Nov. 2015, pp. 1–5.
[31] C. Oestges, "Validity of the Kronecker model for MIMO correlated channels," in *Proc. IEEE 63rd Veh. Technol. Conf.*, vol. 6. May 2006, pp. 2818–2822.
[32] X. Chen, "Throughput multiplexing efficiency for MIMO antenna characterization," *IEEE Antennas Wireless Propag. Lett.*, vol. 12, pp. 1208–1211, 2013.

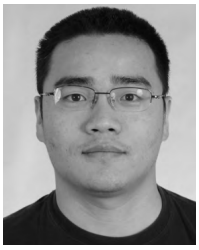

WEI FAN received the B.E. degree from the Harbin Institute of Technology, China, in 2009, the double master's degree (Hons.) from the Politecnico di Torino, Italy, and the Grenoble Institute of Technology, France, in 2011, and the Ph.D. degree from Aalborg University, Denmark, in 2014. In 2011, he was with Intel Mobile Communications, Denmark, as a Research Intern. He conducted a three-month internship at Anite Telecoms Oy, Finland, in 2014. He is currently an Associate Professor with the Antennas, Propagation and Millimeter-wave Systems Section, Aalborg University. His main areas of research are over-the-air testing of multiple antenna systems, radio channel sounding, modeling, and emulation.

PEKKA KYÖSTI received the M.Sc. degree in mathematics from the University of Oulu, Finland. From 1998 to 2002, he was with Nokia Networks. From 2002 to 2016, he was with Elektrobit/Anite. Since 2002, he has been involved in radio channel measurements, estimation, and modeling. From 2008 to 2012, he was actively developing methods for MIMO over-the-air testing. He was moved to Keysight Technologies Finland Oy along the acquisition in 2016. He is currently involved in channel modeling for 5G systems with Keysight Technologies Finland Oy and with the University of Oulu.

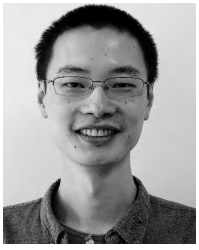

YILIN JI received the bachelor's and master's degrees in wireless communications from Tongji University, China, in 2013 and 2016, respectively. He is currently a Ph.D. Fellow with the Section of Antennas, Propagation and Millimeter-wave Systems Section, Aalborg University. His focus is mainly on antenna array signal processing, channel characterization, and OTA testing.

LASSI HENTILÄ received the M.Sc. degree in telecommunication from the University of Oulu, Finland, in 2004. From 2004 to 2016, he was with Elektrobit/ Anite. Since 2004, he has been involved in radio channel measurements, modeling, and emulation. He moved to Keysight Technologies Finland Oy along the acquisition in 2016. He is currently involved in channel modeling and testing methodology for 5G systems with Keysight Technologies Finland Oy.

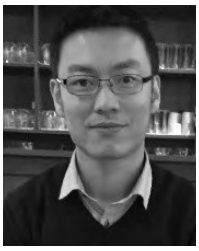

XIAOMING CHEN received the B.Sc. degree in electrical engineering from Northwestern Polytechnical University, Xi'an, China, in 2006, and the M.Sc. and Ph.D. degrees in electrical engineering from the Chalmers University of Technology, Gothenburg, Sweden, in 2007 and 2012, respectively. From 2013 to 2014, he was a Post-Doctoral Researcher with the Chalmers University of Technology. From 2014 to 2017, he was an Antenna Specialist with Qamcom Research and Technology AB, Gothenburg. Since 2017, he has been a Professor with Xi'an Jiaotong University, Xi'an. His research areas include MIMO antennas, over-the-air testing, reverberation chambers, and hardware impairments and mitigation. He serves as an Associate Editor of the IEEE Antennas and Wireless Propagation Letters and is a reviewer of several major IEEE journals. He received the URSI (International Union of Radio Science) Young Scientist Award 2017.

GERT FRØLUND PEDERSEN was born in 1965. He received the B.Sc. degree (Hons.) in electrical engineering from the College of Technology in Dublin, Ireland, in 1991, and the M.Sc. and Ph.D. degrees from Aalborg University in 1993 and 2003, respectively. He has been with Aalborg University since 1993, where he is a Full Professor heading the Antenna, Propagation and Networking Laboratory with 36 researchers. Furthermore, he is also the Head of the Doctoral School on Wireless Communication with some 100 Ph.D. students enrolled. He has authored or co-authored 175 peer-reviewed papers and holds 28 patents. His research has focused on radio communication for mobile terminals especially small antennas, diversity systems, propagation and biological effects. He was also a Consultant for developments of over 100 antennas for mobile terminals, including the first internal antenna for mobile phones in 1994 with lowest SAR, first internal triple-band antenna in 1998 with low SAR and high TRP and TIS, and lately various multiantenna systems rated as the most efficient on the market. He was most of the time with joint university and industry projects and have received over 12*M* in direct research funding. He is currently the Project Leader of the SAFE Project with a total budget of 8*M* investigating tunable front end, including tunable antennas for the future multiband mobile phones. He has been one of the pioneers in establishing over-the-air (OTA) measurement systems. The measurement technique is now well-established for mobile terminals with single antennas and he was chairing the various COST groups (swg2.2 of COST 259, 273, 2100 and now ICT1004) with liaison to 3GPP for OTA test of MIMO terminals. He is currently deeply involved in MIMO OTA measurement.